# Monitoring and Inhibition of Insulin Fibrillation by a Small Organic Fluorogen with Aggregation-Induced Emission Characteristics

Yuning Hong,[†,‡] Luming Meng,[†] Sijie Chen,[#] Chris Wai Tung Leung,[†] Lin-Tai Da,[†] Mahtab Faisal,[†] Daniel-Adriano Silva,[†] Jianzhao Liu,[†] Jacky Wing Yip Lam,[†] Xuhui Huang,*,[†,#] and Ben Zhong Tang*,[†,‡,#]

[†]Department of Chemistry, State Key Laboratory of Molecular Neuroscience, Institute of Molecular Functional Materials, [‡]Nano Science and Technology Program, [#]Division of Biomedical Engineering, The Hong Kong University of Science & Technology, Clear Water Bay, Kowloon, Hong Kong, China

S *Supporting Information*

ABSTRACT: Amyloid fibrillation of proteins is associated with a great variety of pathologic conditions. Development of new molecules that can monitor amyloidosis kinetics and inhibit fibril formation is of great diagnostic and therapeutic value. In this work, we have developed a biocompatible molecule that functions as an *ex situ* monitor and an *in situ* inhibitor for protein fibrillation, using insulin as a model protein. 1,2-Bis[4-(3-sulfonatopropoxyl)phenyl]-1,2-diphenylethene salt (BSPOTPE) is nonemissive when it is dissolved with native insulin in an incubation buffer but starts to fluoresce when it is mixed with preformed insulin fibril,

enabling *ex situ* monitoring of amyloidogenesis kinetics and high-contrast fluorescence imaging of protein fibrils. Premixing BSPOTPE with insulin, on the other hand, inhibits the nucleation process and impedes the protofibril formation. Increasing the dose of BSPOTPE boosts its inhibitory potency. Theoretical modeling using molecular dynamics simulations and docking reveals that BSPOTPE is prone to binding to partially unfolded insulin through hydrophobic interaction of the phenyl rings of BSPOTPE with the exposed hydrophobic residues of insulin. Such binding is assumed to have stabilized the partially unfolded insulin and obstructed the formation of the critical oligomeric species in the protein fibrillogenesis process.
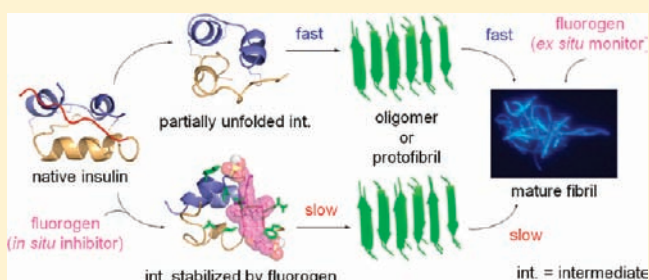
■ INTRODUCTION

Amyloidal fibrils are insoluble protein aggregates, an excessive accumulation of which in organs and tissues can lead to biological dysfunctions and result in pathologic symptoms.[1−5] Protein misfolding and aggregation into amyloidal fibrils have been regarded as the hallmarks of a large variety of debilitating disorders: Alzheimer's, Parkinson's and Huntington's diseases, spongiform encephalopathy, type II diabetes, cardiac arrhythmias, rheumatoid arthritis, atherosclerosis, prolactinomas, and polyneuropathy, among others.[6−9] Undoubtedly, sensitive detection of the protein tangles and plaques and mechanistic understanding of the amyloid deposition processes in molecular detail are of diagnostic importance and have therapeutic implications.

Insulin is a protein that readily undergoes the fibrillogenesis process and has been an excellent model for studying protein amyloidogenesis.[10] Insulin fibrils are often formed at the sites of frequent insulin injections,[11] which has been categorized as one of the amyloidal diseases. Serum samples from patients with Parkinson's disease symptoms have been found to show an autoimmune response to insulin oligomers and fibrils, suggestive of possible involvement of the insulin aggregates in the neurodegenerative disease.[12] Moreover, fibril formation has been a confounded nuisance to long-distance shipping and long-term storage of insulin.[13,14] Understanding the molecular

basis of insulin aggregation is thus of great value to modeling amyloidogenesis processes and to improving delivery systems for diabetes treatment.

Insulin is a 51-residue hormone involved in the homeostasis of blood glucose levels. It is composed of two peptide chains (A and B) with 21 and 30 amino acid residues, respectively (Figure 1).[15] Insulin adopts a primarily helical structure in the native state, in which residues A1−A8 and A13−A20 form two helices in the A chain (A1 and A2 helixes, respectively), while residues B11−B19 form a helix in the B chain (B helix). Insulin can form amyloidal fibrils *in vitro* under certain destabilizing conditions, such as high temperature, low pH, increased ionic strength, exposure to hydrophobic surface, and shaking and stirring.[16] Although it is still under debate whether an intermolecular hydrophobic effect or electrostatic attraction is the driving force for amyloidogenesis,[17,18] it is generally recognized that fibrillogenesis is initiated with the partial unfolding of the insulin monomers, followed by their further association into protein oligomers and amyloid aggregates rich in *β*-sheet structure.[19,20]

To investigate protein amyloidogenesis, many spectroscopic and microscopic techniques have been employed, including
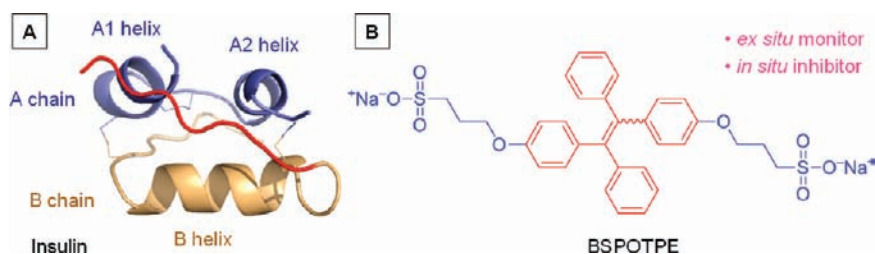
Figure 1. (A) Crystal structure of bovine insulin (PDB ID: 2ZP6). Insulin is composed of two peptide chains (A and B), in which residues A1−A8 and A13−A20 form two helices in the A chain (A1 and A2 helices, respectively), residues B11−B19 form a helix in the B chain (B helix), and residues B23−B30 form a flexible tail (denoted by a red line). (B) Structure of 1,2-bis[4-(3-sulfonatopropoxy)phenyl]-1,2-diphenylethene sodium salt (BSPOTPE), which plays dual roles (*ex situ* monitor and *in situ* inhibitor) in the insulin fibrillogenesis process.

fluorescence spectroscopy, nuclear magnetic resonance, scanning electron microscopy (SEM), atomic force microscopy, real-time light scattering, stopped-flow turbidimetry, X-ray diffraction, circular dichroism (CD), positron emission tomography, and single-photon emission computed tomography.[21−28] Among the techniques, fluorescence is superior in terms of simplicity and rapidity. Whereas attempts have been made to utilize the intrinsic fluorescence of proteins, such emission is normally weak in intensity and short in wavelength (often in the UV region).[29] Utilization of the fluorescence technique thus critically depends on the development of efficient extrinsic fluorophores.

Thanks to the enthusiastic efforts of scientists in the area of research, a series of extrinsic fluorophores have been developed, such as thioflavin T (ThT),[26−28] Michler's hydrol blue, difluoroboron derivatives, rhodamine analogues, conjugated oligothiophenes, and semiconductor quantum dots.[30−38] ThT has been a standard probe for amyloid assay for about half a century. Despite its widespread use, it suffers from a number of drawbacks, such as small Stokes shift, low specificity, poor sensitivity, false-positive response, poor reliability, incapability of catching oligomeric intermediates, and unsuitability for kinetic study. Owing to its twisted intramolecular charge-transfer character, its fluorescence in an aqueous medium or polar environment is unsatisfactorily weak.

Similar to ThT, many of the other fluorophores mentioned above also contain electron donors and acceptors, between which intramolecular charge transfer occurs.[31] Such fluorophores are sensitive to hydrophobicity of the environment, and their emissions are intensified upon binding to hydrophobic regions of amyloids rich in β-sheet structure. However, when multiple fluorophore molecules are accumulated in a hydrophobic patch of protein, π−π interaction between their stacked aromatic rings occurs, which promotes the formation of such detrimental species as excimers and exciplexes. This can lead to severe emission self-quenching, making the fluorophores unsuitable for quantitative analysis.[39]

We have recently discovered a group of propeller-shaped luminogens that are nonemissive when they are molecularly dissolved but become highly luminescent when they are supramolecularly aggregated.[39] We coined the term "aggregation-induced emission" (AIE) for this unusual photophysical effect and proposed restriction of intramolecular rotation (RIR) as the mechanistic cause for the AIE phenomenon.[40−42] The AIE effect seems ideally suited for the study of protein fibrillogenesis, for both of them are associated with aggregate formation. A water-miscible AIE luminogen may work as an excellent amyloidal probe because (i) it is nonemissive in an aqueous buffer and thus the interference from background

emission is minimal, (ii) its aromatic core may facilitate its docking on the hydrophobic surface of insulin aggregates, hence activating the RIR process and switching on its light emission, and (iii) its emission intensity may be increased to varying extents in the nucleation, elongation, and equilibrium phases, thereby enabling the evaluation of amyloidogenesis kinetics.

Tetraphenylethene (TPE) is an iconic AIE luminogen. It can be easily prepared and readily modified or functionalized. Due to the synthetic advantage, a large variety of TPE derivatives have been created and investigated as AIE bioprobes in recent years.[40,42] In this work, a water-miscible TPE salt named sodium 1,2-bis[4-(3-sulfonatopropoxy)phenyl]-1,2-diphenylethene (BSPOTPE; Figure 1B) is chosen as a model compound to explore the potential applications of AIE luminogens for amyloidogenesis study. Thanks to its excellent solubility in water, BSPOTPE is nonfluorescent in physiological buffers. It remains weakly fluorescent in the presence of native insulin but becomes emissive when admixed with preformed insulin fibrils. In this paper, we demonstrate that BSPOTPE can discriminate between native and fibrillar forms of insulin and can work as an *ex situ* bioprobe for quantitative analysis and kinetics study of amyloidal fibril formation.

In the area of amyloidosis research, scientists have devoted much effort to identify external inhibitors for fibril formation.[43,44] Inhibition of fibril assembly is a strategy for therapeutic intervention to prevent proteins from aggregating.[45,46] A number of substances have been found to interfere with amyloidosis processes. It has been reported that peptides, biopolymers, and nanoparticles can perturb fibrillation processes *in vitro*,[9,47−49] while metallic complexes and quantum dots can retard proteins from forming amyloid fibrils.[50−52] Peptides, however, can be easily digested *in vivo*. Nontrivial protections through structural modifications are thus needed for them to function as inhibitors under physiological conditions.[53,54] Big polymers have difficulty penetrating the blood−brain barrier, while inorganic nanoparticles are often toxic. These drawbacks make it less feasible to develop these materials into viable therapeutic agents or drugs.

Small organic molecules, on the other hand, offer the potential to overcome the thorny difficulties encountered by the materials discussed above through rational structural design.[9,43,55−60] Various organic inhibitors have been developed so far, most of which are derivatives of amyloid fibril-binding dyes such as ThT. Owing to this structural feature, these inhibitors generally function through targeting the fibril form of proteins.[61,25] Recent advances in the area, however, indicate that the most toxic form of amyloid protein is the nonfibrillar and oligomeric species.[62,63] The partial unfolding of monomers

is the critical step before they undergo nucleation to form oligomeric species and further association into amyloidal aggregates. Targeting the partially unfolded conformations of proteins may thus be an effective way to inhibit the nucleation process that leads to the formation of toxic oligomers or protofibrils.

Our previous study has revealed that BSPOTPE is prone to binding to molten globule intermediates formed in the unfolding processes of proteins.[40,64] This inspires us to examine whether BSPOTPE will interfere with amyloidogenesis of insulin. In this paper, we show that BSPOTPE can indeed affect the insulin fibrillogenesis under low pH at high temperature. *In situ* mixing of BSPOTPE with insulin in an incubation buffer impedes nucleation and elongation processes of the latter. The extent of inhibition is found to be proportional to the dose of BSPOTPE added to the aqueous mixture. Only a small inhibitor-to-protein (I/P) ratio of 1:5 (or 20%) is needed to inhibit the insulin fibrillogenesis, in contrast to other small-molecule or short-peptide inhibitors, whose I/P ratios are generally $\geq$100%.[47,59,60] Theoretical modeling suggests that BSPOTPE binds tightly to the partially unfolded form of insulin, instead of its native form, via hydrophobic interaction. This binding may have obstructed the oligomer formation and slowed the nucleation process.

RESULTS AND DISCUSSION

BSPOTPE as *ex Situ* Probe for Monitoring Insulin Amyloidogenesis. BSPOTPE was prepared by the synthetic procedures reported in our previous paper.[65] The luminogen is AIE active: its fluorescence quantum yield (Φ_F) is increased from 0.37% in water (a molecular solution) to 17.5% in acetonitrile (an aggregate suspension), with an α_{AIE} value of 47.3.[40] As can be seen from the photoluminescence (PL) spectrum shown in Figure 2A, the dilute solution of BSPOTPE
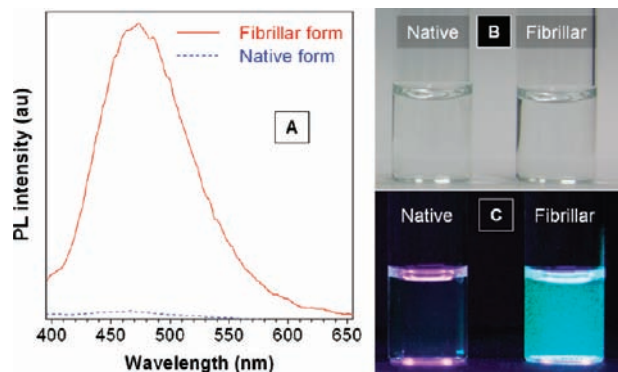
Figure 2. (A) PL spectra of BSPOTPE in the presence of native and fibrillar forms of bovine insulin. The amyloid fibrils were obtained by heating an insulin solution in a pH 1.6 buffer at 65 °C for 20 h. PL measurements were performed in a pH 7 buffer at [BSPOTPE] = 5 μM, [insulin] = 5 μM, and λ_{ex} = 350 nm. Photographs of mixtures of BSPOTPE with native and fibrillar forms of insulin taken under (B) normal laboratory lighting and (C) illumination with a UV light of 365 nm.

remains nonemissive after the addition of native bovine insulin in phosphate-buffered saline (PBS). Its fluorescence is switched on when a small amount of fibrillar insulin is added to the BSPOTPE solution. The fluorescence intensity does not change much over a wide range of pH values (1−9) and a large span of salt concentrations (10^{-6}−1 M; Figure S1,

Supporting Information). Likewise, the fluorescence intensity of BSPOTPE changes little with variations in the pH value and salt concentration in the absence of insulin. The solutions of BSPOTPE in the presence of both native and fibrillar forms of insulin are transparent under laboratory lighting (Figure 2B). Upon UV photoexcitation, the mixture of fibrillar insulin and BSPOTPE emits a strong green light, while that of native insulin and BSPOTPE emits almost no light (Figure 2C).

The distinct emission behaviors of BSPOTPE in the presence of native and fibrillar forms of insulin prompted us to explore the possibility of utilizing it to monitor the kinetic process of amyloid fibrosis. We dissolved a commercial product of insulin powder in a HCl/NaCl buffer (pH 1.6) at room temperature and then incubated the resultant solution at 65 °C (Scheme S1, Supporting Information). The use of the acidic buffer and high temperature is to accelerate the fibril growth, noting that pharmaceutical insulin products can suddenly form aggregates upon perturbations with thermal shock, mechanical agitation, etc. during their shipping, handling, and delivery processes. A small aliquot of the incubation mixture was taken out at a defined time, cooled to room temperature, and diluted with a large amount of PBS to neutral condition. BSPOTPE was added to the resultant mixture prior to PL measurement. As shown in Figure 3A, no PL signal is recorded when the
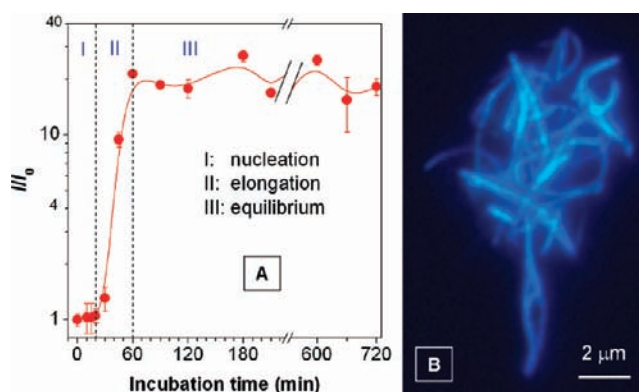
Figure 3. (A) Insulin fibrillogenesis process monitored by BSPOTPE bioprobe. PL measurements were performed in a pH 7 buffer at [BSPOTPE] = 5 μM, [insulin] = 5 μM, and λ_{ex} = 350 nm. (B) Fluorescence image of the insulin fibrils stained by BSPOTPE.

insulin solution has been incubated for <20 min. The mixture becomes emissive after incubating for 30 min. The PL intensity quickly increases and reaches its maximum at 60 min, with no big change observable afterward.

The data in Figure 3A indicate that the insulin amyloido-genesis process involves three distinct steps: (I) nucleation, (II) elongation, and (III) equilibration.[29] Under the experimental conditions of our work, the initial nucleation occurs in the first 30 min, during which BSPOTPE emits faintly. The nucleation is followed by an exponential elongation onward to 1 h, in which PL of BSPOTPE is rapidly enhanced. After 1 h, the fibril formation reaches the final equilibrium stage, with the PL intensity leveled off in the plateau. When the mature insulin fibrils are taken out from the buffer and stained with BSPOTPE, they become readily visible under a fluorescence microscope (Figure 3B).

Figure 4A shows that PL of BSPOTPE is intensified with an increase in the concentration of fibrillar insulin. The rate of emission enhancement (I/I_0) is fast in the region of low insulin
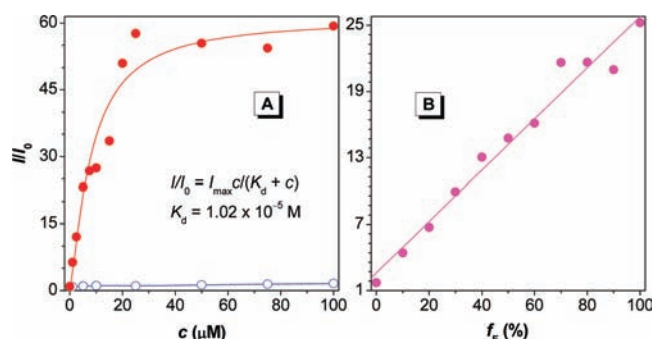
Figure 4. (A) Change in the PL intensity of BSPOTPE at 470 nm with variation in the concentration of fibrillar (solid circles) or native (open circles) insulin. (B) Plot of PL intensity of BSPOTPE in insulin mixture versus molar fraction of fibrillar insulin (f_F). The total protein concentration (5 μM) was kept constant in each run. I_0 is the PL intensity in the absence of insulin, c is the concentration of insulin, and k_d is the dissociation constant; [BSPOTPE] = 5 μM, λ_{ex} = 350 nm.

concentration (c) and becomes slow at $c > 20$ μM. Analysis of the binding isotherm reveals a linear relationship in the region of $c = 0-5$ μM. The binding constant of BSPOTPE to the insulin fibrils is about 10^5 M, comparable to those of the commercial stains for amyloidal fibrils.[66] The PL intensity of BSPOTPE practically does not change with the variation in the concentration of native insulin (0–100 μM; data shown by open circles in Figure 4A). In another set of experiments, a series of insulin mixtures were prepared, in which the fraction of fibrillar insulin (f_F) was changed while the total insulin concentration was kept constant. As shown in Figure 4B, the emission of BSPOTPE increases linearly with increasing f_F, indicating that the AIE luminogen can be used for quantitative assay of fibrillar insulin.

BSPOTPE as *in Situ* Inhibitor for Hindering Insulin Amyloidogenesis. The data presented above prove that BSPOTPE is an excellent *ex situ* bioprobe for detecting insulin fibrils and for monitoring amyloidogenesis kinetics. To check whether the presence of BSPOTPE *in situ* will affect the formation of amyloid fibrils, different doses of BSPOTPE (0–100 μM) were added into insulin solutions (500 μM) prior to warming them to 65 °C (Scheme S1B). Figure 5A shows the time courses of the insulin fibrillogenesis followed by the changes in the PL of BSPOTPE. In comparison to the fibrosis process in the absence of BSPOTPE discussed above, the nucleation phase is prolonged and the growth rate in the elongation phase is decelerated by the presence of BSPOTPE. The nucleation phase characterized by the weak PL is extended from 30 min to 2 h when insulin is premixed with a small dose of BSPOTPE (10 μM). The exponential elongation phase, where the PL intensity increases with the fibril growth, is slowed in rate. To reach the final equilibrium phase, >3 h incubation is required, although it takes only 1 h to arrive at the plateau in the absence of BSPOTPE.

The inhibition effect of BSPOTPE on the amyloidogenesis of insulin becomes more pronounced when the luminogen dose in the incubation solution is increased. Figure 5B shows the correlation between the induction period and the BSPOTPE dose in the insulin incubation buffer. Here, the induction period is defined as the duration of the nucleation phase. The induction period is expanded linearly with increasing BSPOTPE dose. In the presence of 25 and 50 μM concentrations of BSPOTPE, the induction periods of
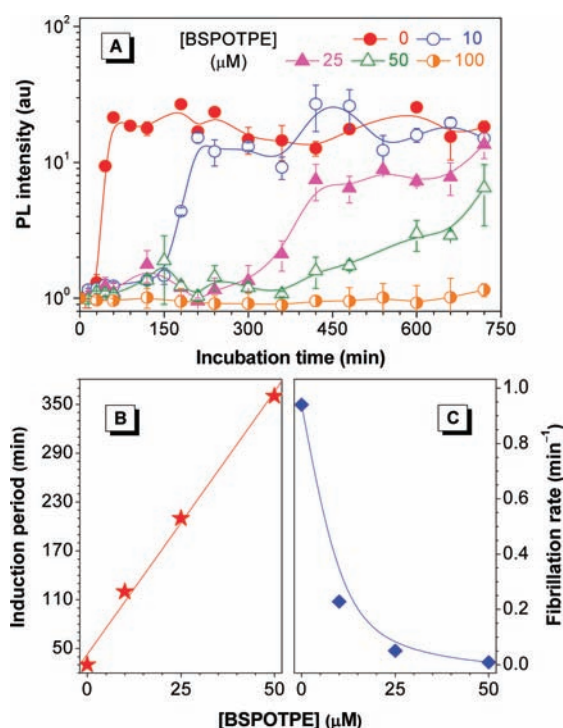

Figure 5. (A) Trajectories of fibrillogenesis of insulin (500 μM) monitored by BSPOTPE at different fluorogen doses (0–100 μM). Plots of changes in (B) induction period and (C) fibrosis rate as a function of fluorogen dose. Insulin was incubated in the BSPOTPE-containing buffers (pH 1.6) at 65 °C. PL spectra were taken using the diluted incubation mixtures under neutral conditions at [insulin] = 5 μM, [BSPOTPE] = 5 μM, and λ_{ex} = 350 nm.

fibrillogenesis are lengthened to 3 and 6 h, respectively. When the BSPOTPE dose is increased to 100 μM, the insulin fibrillogenesis is totally suppressed, with practically no change in the PL intensity observable after 20 h incubation. When the BSPOTPE dose is further increased to equal the amount of the protein (500 μM), fibrils are not formed even after the insulin solution has been incubated for as long as 1 week.

The effects of the inhibitors reported in the literature have been known to be critically dependent on I/P ratios.[48−50,60] A high I/P ratio is normally required to exert an inhibitory effect, for some "inhibitors" actually accelerate, rather than decelerate, fibrosis at low I/P ratios.[49] For example, high I/P ratios of 2:1, 10:1, and >100:1 are required for polyoxometalates,[50] heparin,[48] and curcumin,[60] respectively, to inhibit protein amyloidogenesis. In sharp contrast, a small I/P ratio of 1:5 (or 0.2:1) is sufficient for BSPOTPE to suppress the insulin fibrillogenesis. Increasing the dose of BSPOTPE monotonically enhances its inhibitory potency. As shown in Figure 5C, the fibrillation rate, denoted as the slope of the elongation phase, decreases exponentially when the BSPOTPE dose is increased. These results suggest that BSPOTPE interacts strongly with the protein, which interferes with the unfolding and denaturing process of native insulin.

We used far-UV CD spectroscopy to follow the amyloidogenesis of insulin by monitoring the changes in its secondary structure.[67,68] The native insulin in the PBS buffer shows an α-helix-rich CD pattern with two negative Cotton effects at 209 and 220 nm (Figure 6A), in agreement with its crystal structure extracted from the Protein Data Bank (PDB).[10] While the spectral profile remains almost unchanged in the first 30 min,
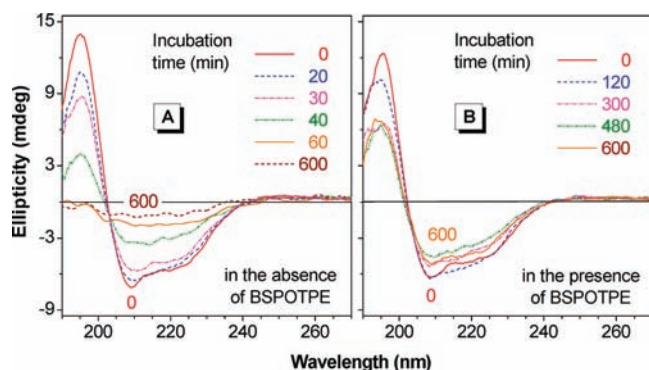
1683

dx.doi.org/10.1021/ja208720a | *J. Am. Chem. Soc.* 2012, 134, 1680−1689

Figure 6. CD spectra of insulin incubated in the (A) absence and (B) presence of BSPOTPE (100 μM) in a pH 1.6 buffer at 65 °C for different periods of time (0–600 min).

the Cotton effects are weakened in intensity. This suggests that the secondary structure of insulin is partially perturbed in the nucleation phase.[64] After 40 min incubation, the CD spectrum is changed from an α-helical-rich profile to a β-sheet-rich one, as suggested by the emergence of a new CD band at 218 nm. The β-sheet-rich structure remains nearly unchanged over a period of 10 h. Incubation of insulin in the presence of BSPOTPE slows its transformation from α-helical- to β-sheet-rich structure (Figure S2, Supporting Information). When 100 μM BSPOTPE is added to the incubation solution of insulin, no big spectral change is observed, even after the solution has been heated for 10 h (Figure 6B). The time courses of the changes in the ellipticity are consistent with those in the emission intensity (cf., Figure S2D and Figure 5A).

Imaging by SEM further verifies the above observations. In the absence of BSPOTPE, numerous amyloidal fibrils with diameters of about 20 nm are formed after the insulin solution has been incubated for 1 h (Figure 7A). In the presence of
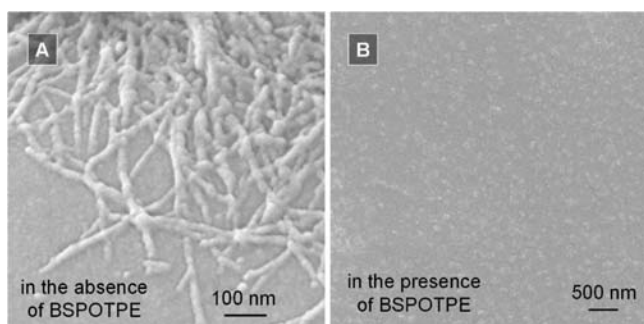

Figure 7. SEM images of morphologies of insulin after incubation in the (A) absence and (B) presence of BSPOTPE (50 μM) in a pH 1.6 buffer at 65 °C for (A) 1 h and (B) 2 h.

BSPOTPE, however, only spherical particles but not elongated fibrils are formed, even after the solution has been incubated for 2 h under similar conditions (Figure 7B), implying that the insulin amyloidogenesis is still circumscribed in the nucleation phase. The SEM results here and the CD data discussed above corroborate that BSPOTPE is an excellent indicator for monitoring the progress of insulin fibrillogenesis.

To further evaluate the inhibition effect of BSPOTPE on the amyloidogenesis, additional experiments were conducted where BSPOTPE was added to the insulin solution at different times of incubation (t_a) during the process of insulin fibrillation. As

shown in Figure 8A, the addition of BSPOTPE prior to the thermal treatment ($t_a = 0$) induces a great inhibition effect, as
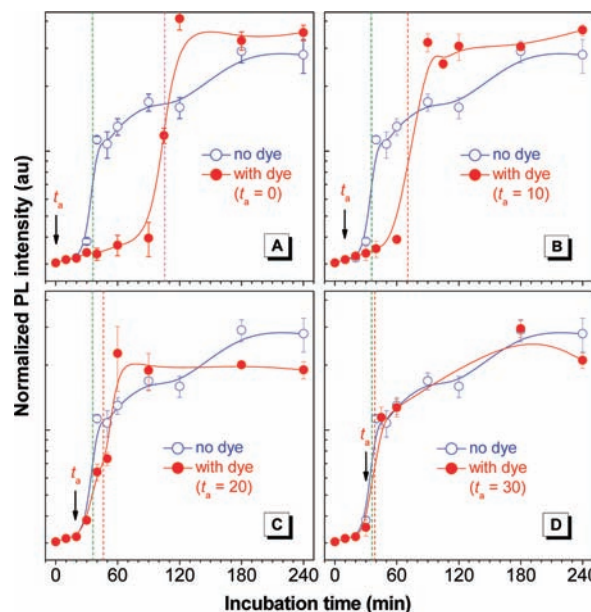

Figure 8. Effect of BSPOTPE on fibrillogensis kinetics of insulin. BSPOTPE (10 μM) was added to the buffer solutions (pH 1.6) of insulin (500 μM) at 65 °C at different incubation times (t_a): (A) 0, (B) 10, (C) 20, and (D) 30 min. The dashed lines indicate the estimated half-times ($t_{1/2}$) of the insulin fibrillation.

evidenced by the large right-shift of the fibrillation curve of insulin in the presence of BSPOTPE relative to that in the absence of the luminogen. When BSPOTPE is added after the insulin solution has been incubated at 65 °C for 10 min, it still exerts a readily recognizable inhibitory effect on the insulin fibrillation (Figure 8B). Addition of BSPOTPE after 20 min of incubation causes only a small inhibition effect, whereas almost no effect is observed when BSPOTPE is added after 30 min of incubation, as evidenced by the virtual overlap of the fibrillation curves in the presence and absence of the luminogen (Figure 8D).

A half-time ($t_{1/2}$) is defined here as the time for the PL intensity of PSPOTPE to reach half the height of the plateau in the insulin fibrillation curve. When BSPOTPE is added to the incubation solution at 0, 10, and 20 min, the corresponding $t_{1/2}$ values are ∼105, ∼70, and ∼45 min (panels A−C in Figure 8), revealing an inverse relationship between t_a and $t_{1/2}$. When BSPOTPE is added at $t_a = 30$ min, the $t_{1/2}$ value becomes almost identical to that in the absence of BSPOTPE (Figure 8D), indicating that the addition of BSPOTPE to the insulin solution at this stage has no effect on the protein fibrillogenesis. These results imply that the insulin fibrillogenesis can be inhibited only when BSPOTPE is added in the nucleation phase before the oligomers are formed. We hypothesize that the binding of the BSPOTPE molecules to the partially unfolded insulin chains has obstructed the proteins from aggregating into oligomeric and protofibrillar species. In other words, no inhibition effect can be expected if BSPOTPE is added after the critical nuclei have formed. To verify the validity of this hypothesis, molecular dynamics (MD) simulations and large-scale docking are performed to learn how BSPOTPE inhibits insulin amyloidogenesis at the molecular level.

Mechanisms for BSPOTPE's Dual Roles as *ex Situ* Probe and *in Situ* Inhibitor. Our experimental results clearly show that BSPOTPE plays two different roles in the process of insulin amyloidogenesis. The question is, what is the molecular mechanism for the luminogen to function as both an *ex situ* probe and an *in situ* inhibitor? Specifically, the following questions need to be properly answered in the mechanistic study: (1) why does BSPOTPE show distinct PL responses toward the native and fibrillar forms of insulin, and (2) how does BSPOTPE inhibit the nucleation process of insulin and suppress its fibrillation process?

The working principle of BSPOTPE as an *ex situ* probe for insulin fibrillation is directly associated with its unusual AIE characteristics. Our previous studies have shown that RIR is the main mechanistic cause for the AIE phenomenon.[40−42] BSPOTPE is an AIE luminogen with excellent water solubility. In its dilute solution in water, BSPOTPE exists as isolated species. The dynamic rotational or torsional motions of its phenyl rotors effectively annihilate its excited states, thus rendering the luminogen nonemissive in the solution state. Upon aggregate formation, such motions become physically restricted, which effectively blocks the nonradiative relaxation channels and populates the radiative decays of the excitons, thereby making its aggregates highly luminescent.[40−42]

Bovine insulin has an isoelectric point of pH 5.6 and carries a net negative charge at pH 7. BSPOTPE is also negatively charged under neutral conditions. Electrostatic repulsion between the same charges should hinder BSPOTPE from binding to insulin. Since the hydrophobic residues of insulin are buried in the inner core of its native folding structure, it is difficult for BSPOTPE to engage in hydrophobic interaction with the native protein. BSPOTPE thus remains isolated and hence nonemissive in the solution of native insulin. In the insulin fibrils, however, extended β-strand structures are assembled through hydrophobic interaction. BSPOTPE luminogen contains multiple phenyl rings and may stack on the surface of the β-strand structure through hydrophobic interaction. The noncovalent binding to the insulin fibrils activates the RIR process and thus causes the luminogen to fluoresce (Scheme 1).

Scheme 1. Proposed Mechanistic Diagrams for the Dual Functions of BSPOTPE as *ex Situ* Monitor and *in Situ* Inhibitor in the Process of Insulin Amyloidogenesis
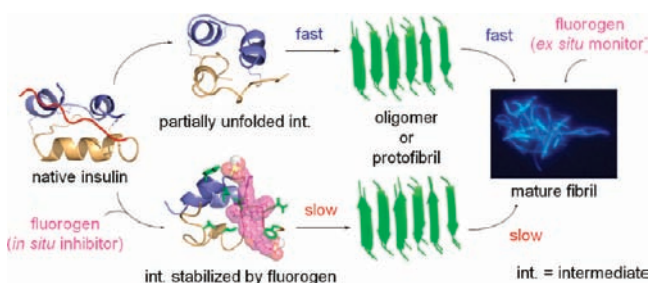
Previous study revealed that partial unfolding of native protein is an indispensible step in the process of protein amyloidogenesis.[19] We speculate that BSPOTPE may have bound to such a partially unfolded insulin structure, delayed the nucleation step, and decelerated the fibril formation. To gain mechanistic insight into the binding process of BSPOTPE to insulin, MD simulations and docking calculations were performed (Scheme S2, Supporting Information). The simulations were carried out under two sets of conditions: pH 7, T = 300 K and pH <2 (low pH), T = 340 K, to mimic the two experimental settings for native and fibril forms of insulin, respectively. To search out possible binding modes, a large-scale flexible docking between BSPOTPE and an ensemble of the protein structures under both conditions obtained from the MD and replica exchange molecular dynamics (REMD) simulations was conducted (Figures S3−S7, Supporting Information). Under each condition, 1000 docking conformations were generated for each of 100 protein structures, with a total of 100,000 docking poses.[69,70]

Without BSPOTPE, insulin is stable under the native conditions with root-mean-square displacement (rmsd) below 3.5 Å in our theoretical simulations (Figure S3). Under the fibril-forming conditions, however, insulin undergoes partial unfolding with rmsd up to 5.0 Å, especially in the B-chain helix region (Figures S3−S5). The lowest docking scores are plotted in Figure 9 against the solvent-accessible surface areas of
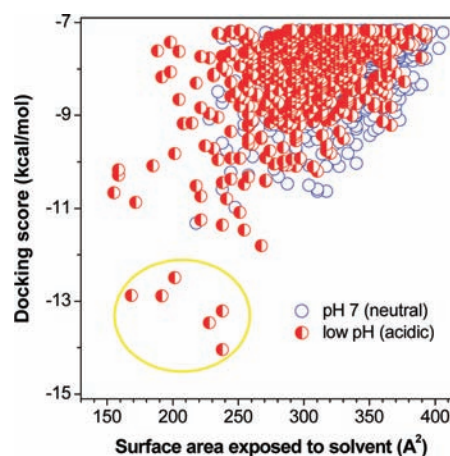

Figure 9. Plot of the surface area of BSPOTPE exposed to solvent versus the docking score upon its docking to the native (pH 7; open blue circles) or partially unfolded (low pH; half-filled red circles) form of insulin. With a decrease in the solvent-accessible surface area, the docking score (in terms of energy) is lowered, indicating better docking with BSPOTPE embedded in insulin. Under each condition, the docking poses with energies lower than −7 kcal/mol selected from a total of 100,000 docking poses are plotted.

BSPOTPE under the two different conditions. Among all the docking poses, the nine poses with the lowest energies are all realized under the fibril-forming conditions. Moreover, the lowest docking energy under the fibril-forming conditions (−14.04 kcal/mol) is substantially lower than that under the native conditions (−11.32 kcal/mol). These results indicate that BSPOTPE binds more favorably to the partially unfolded insulin, in comparison to its native form. As can be seen from Figure 9, the docking energies also show a strong correlation with the surface areas of BSPOTPE that are exposed to the solvent.

Further inspection of the docking conformations with the lowest energies reveals that the hydrophobic interaction stabilizes the BSPOTPE−insulin conjugate. As shown in Figure 10, the six top binding poses with the lowest energies all display a common structural feature: the phenyl rings of BSPOTPE are in contact with the hydrophobic residues of insulin, such as leucine, valine, phenylalanine, and tyrosine. Under the fibril-forming conditions, the B-chain helix (B11−B19) of insulin is
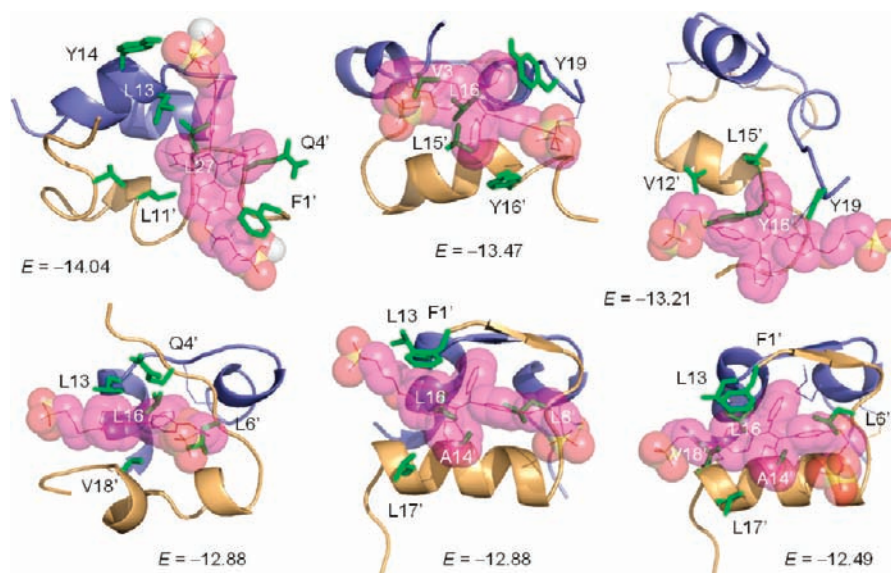
Figure 10. The six best docking poses with the lowest binding free energies (E; kcal/mol) at low pH. BSPOTPE is shown in a sphere representation with a color scheme of magenta for carbon, red for oxygen, and yellow for sulfur, while insulin is shown in a surface representation with a color scheme of blue for A chain and gold for B chain. The residues interacting with BSPOTPE are shown as sticks with hydrogen atoms omitted for clarity (residues labeled with primes are from the B chain).

partially unfolded, with a large structural flexibility. This enhances the probability of exposure of its hydrophobic residues to solvent, which in turn encourages the binding of BSPOTPE through hydrophobic interaction (see the representative docking conformations shown in Figure S7). Previous biophysical investigations suggest that this B-chain helix is involved in the nucleation phase of protein fibrillogenesis.[10,71] The binding of BSPOTPE to this segment thus may hamper the nucleus formation, offering a different mechanistic approach to inhibiting protein amyloidogenesis.[44,72,73]

It has been reported that Congo red (CR), a well-known amyloidogenesis inhibitor, prefers to align on the B19−B30 segment of insulin, the flexible tail in the B chain (represented by the red line in Figure 1A).[72] The binding of CR to the insulin monomer may have somehow stabilized the helix and promoted formation of the antiparallel homodimer of insulin. BSPOTPE, on the other hand, has a lower affinity to the native form of insulin. It prefers to bind to the partially unfolded insulin chain with its hydrophobic residues exposed. This binding stabilizes the partially unfolded structure, hampers the nuclei formation, and inhibits the further assembly into fibrillar aggregates (Scheme 1). Since BSPOTPE does not bind to the native insulin, it may not interfere with the biological functions of the protein. In addition to directly inhibiting the fibril nucleation by binding to the on-pathway intermediate states, BSPOTPE may also bind to and stabilize the off-pathway intermediates to prevent the fibrillogenesis from propagating.

CONCLUDING REMARKS

Protein aggregation into amyloidal fibrils is an essential process leading to many neurodegenerative as well as non-neuropathic diseases. In this work, we have developed a water-soluble, biocompatible AIE luminogen into an *ex situ* monitor and an *in situ* inhibitor for protein amyloidogenesis using insulin as a model protein. BSPOTPE emits weakly and strongly in the absence and in the presence of preformed insulin fibrils, respectively, which enables kinetic monitoring of the protein fibrillogenesis. The *in situ* addition of BSPOTPE into the

incubation solution of insulin, on the other hand, inhibits the nucleation phase and slows the elongation process. The extent of the inhibition effect is proportional to the dose of the luminogen. As a fluorescent *ex situ* monitor, the AIE luminogen does not suffer from self-quenching and is resistant to photobleaching,[40−42] while as an anti-amyloid *in situ* inhibitor, a low dose (I/P ≈ 0.2) is sufficient to suppress the amyloid fibrillation. The utilization of amphiphilic AIE luminogen thus offers a new strategy for the development of new diagnostic reagents and therapeutic drugs for monitoring and treatment of the diseases associated with conformational disorders of proteins.

EXPERIMENTAL SECTION

Materials and Sample Preparation. All the reagents (chemicals, solvents, etc.) used in this study were purchased from Aldrich unless otherwise specified. BSPOTPE was prepared according to our published procedures.[65] Bovine insulin was purchased from Sigma-Aldrich and used as received. PBS buffer with pH 7 was purchased from Merck. Water was purified using a Millipore filtration system.

Bovine insulin powder was dissolved in a 25 mM NaCl/HCl solution (pH 1.6). The solution was passed through a 0.45 μm filter and its concentration was determined by measuring its absorbance at 278 nm. The stock solution of BSPOTPE with a concentration of 1.0 mM was prepared by dissolving an appropriate amount of the luminogen in a PBS buffer (pH 7). Insulin fibrils were prepared by incubating the protein solution (500 μM) in the acidic buffer (pH 1.6) at 65 °C (Scheme S1, Supporting Information).

In the study of using BSPOTPE as an *ex situ* probe, an aliquot of the insulin solution taken out from the incubation mixture at a defined time was diluted with PBS (to pH 7.39), followed by the addition of the luminogen. The final concentrations of insulin and BSPOTPE were both 5 μM. The fibril samples were ultrasonicated for at least 10 min prior to PL measurement to avoid sedimentation of large fibrillar aggregates. In the study of using BSPOTPE as an *in situ* inhibitor, the luminogen was added to insulin solution prior to incubating at 65 °C (Scheme S1). An appropriate amount of BSPOTPE was added to the PBS-diluted mixture to keep the luminogen concentration constant (5 μM) before PL measurement.

Instrumentations. Absorption spectra were measured on a Milton Roy Spectronic 3000 array spectrophotometer and emission spectra were recorded on a Perkin-Elmer LS 55 spectrofluorometer with a xenon discharge lamp excitation. Fluorescence assays were performed in a 96-well microtiter plate measured by a Perkin-Elmer Victor[3] multitask plate reader using 355 and 460 nm as excitation and emission wavelengths, respectively. CD spectra were recorded on a Jasco J-810 spectropolarimeter in a 1 mm quartz cuvette using a step resolution of 0.2 nm, a scan speed of 100 nm/min, a sensitivity of 0.1°, and a response time of 0.5 s. Each spectrum was the average of three scans.

Morphologies of the insulin fibrils were imaged on a JEOL 6700F electronic microscope. The aliquot taken out at a defined time of incubation was diluted by pure water, followed by centrifugation (Eppendorf 5415D). The supernatant was removed to avoid the interference from the inorganic salts in the buffer. SEM samples were prepared by drop-casting a dilute insulin solution or suspension onto a copper 400-mesh carrier grid covered with carbon-coated Formvar film. The solvent was removed by evaporation at room temperature in open air.

Fluorescence micrographs were taken on an upright fluorescence microscope (Olympus BX41) using a combination of excitation and emission filters (λ_{ex} = 330−380 nm, diachronic mirror = 400 nm). Samples were prepared by drop-casting the solutions containing insulin fibrils and BSPOTPE onto the microscope slides covered by microscope glasses. The fluorescence images were captured using a computer-controlled SPOT RT SE 18 Mono charge-coupled device (CCD) camera.

Theoretical Modeling. Our simulation methodology comprised two steps: first, MD and REMD[74,75] simulations of insulin were run to widely explore protein conformational spaces and next, representative conformations from the simulations were selected and then docked with BSPOTPE molecules (Scheme S2, Supporting Information). The docking poses with lowest energies served as our predicted binding structures. In order to compare with the experimental results, the simulations were performed under two different sets of conditions: the native conditions of neutral pH and T = 300 K, and the fibril-forming conditions of low pH and T = 340 K.

Bovine insulin (PDB ID: 2ZP6) was chosen as the initial structure. Since it is known that its B-chain C-terminal tail is not critical for fibril formation,[16] the tail was removed in our simulations under both native and fibrillar conditions to speed conformational sampling of the partially unfolded structures. The C-terminal carboxyl groups and all the Glu and His residues were set to be protonated to simulate the protein structures under the fibril forming condition. Due to the lack of force field parameters for protonated C-terminal carboxyl groups, the force field for the C-terminal residues was reparameterized: the partial charges were taken from the Mulliken charges from HF[76−78] 6-31G calculations with Gaussian 03 package,[79] and the bonding and van der Waals parameters were directly taken from the Amber 99SB force field.[80]

MD and REMD Simulations. The MD simulations were run with Amber 99SB force field[80] using GROMACS simulation package.[81] Insulin was first solvated in a water box with 3699 TIP3P waters[82] and 3 sodium counterions to neutralize the system. All the simulations were performed under the NPT ensemble (1.0 bar and 300 K) with coupling constant 0.5 ps^{-1} for Berendsen pressure coupling[83] and 0.1 ps^{-1} for temperature of velocity rescaling thermostat.[84] The cutoff method was used for van der Waals interaction with a radius of 10 Å. For coulomb interaction, Particle Mesh Ewald[85,86] was used to calculate the long-range electrostatic potential, and the radius for the short range was set at 10 Å. Neighbor lists were updated every 20 steps. LINCS[87] was used to constrain all the covalent bonds involving hydrogen atoms. A 1000-step energy minimization was first performed using the steepest descent method. The solvent was then relaxed by applying a restrain potential on protein heavy atoms for 200 ps. Under the native condition, a 50 ns simulation was performed for production.

Under the fibril-forming conditions of high temperature and low pH, insulin was supposed to undergo conformational changes and to partially unfold. Since the conventional MD simulations may suffer from inadequate conformational sampling by being trapped in certain free energy minimums, REMD simulations were thus performed in this work to enhance sampling, for REMD can help the system to escape from the local free energy minimums by inducing a random walk in temperature.[74,75,88] In REMD, the conformations sampled at high temperatures can be exchanged to lower temperatures to enhance sampling because the free energy landscape is flatter at high temperatures. In this algorithm, multiple replicas of simulations are run simultaneously under different temperatures, and the replicas at neighbor temperatures are exchanged according to a well-defined probability that satisfies the detailed balance:

$$P(T_1 \leftrightarrow T_2) = \min\left(1, \exp\left[\left(\frac{1}{k_B T_1} - \frac{1}{k_B T_2}\right)(E_1 - E_2)\right]\right)$$

where T_1 and T_2 are temperatures and E_1 and E_2 are the instantaneous potential energies of neighboring replicas 1 and 2, respectively. After exchanging successfully, the velocities were scaled by a factor of $(((T_1)/(T_2))^{1/2})^{\pm 1}$. A temperature list of 335, 340, 345, 350, 355, 360, 365, 370, 375, 381, 386, 391, and 403 K was used with the exchange time interval set as 2 ps. All the REMD simulations were performed in NVT ensemble with a length of 50 ns for each replica.

Representative Conformations and Docking Calculations. For the 340 K replica of the REMD simulations under the fibril-forming conditions, the first 20 ns was truncated to ensure the equilibrium of the system. The remaining conformations were divided into 100 clusters based on k-center clustering algorithms.[89] During the clustering process, the distance between a pair of conformations is defined as the rmsd of backbone atoms in the B-chain helix (see Figure S5A, Supporting Information, for representative conformations from those clusters with >1% population). For the MD simulation under native conditions, 100 conformations were randomly selected, as insulin does not undergo any significant conformational changes under such conditions.

Rosetta package[90−92] was used to perform the docking between BSPOTPE and insulin. Five structures of BSPOTPE with different orientations of its hydrophilic tails and hydrophobic phenyl rings were first selected (Figure S6, Supporting Information). Energy minimizations on these five initial structures were then performed using HF with a basis set of 6-31G(d) in the Gaussian 03 package.[79] To be consistent with the previous studies,[91] the partial charges obtained from AM1BCC[93,94] were used as the inputs in the Rosetta scoring functions. Since the B-chain helix is known to be important for nucleation in the fibril formation,[10] docking in proximity of this segment was performed to study how BSPOTPE inhibits fibrillation. Specifically, the docking sites were uniformly chosen within 5 Å of two B-chain helix atoms: C_α atoms of Leu32 and Typ37. Under fibril forming condition, since there is a strong correlation for dynamics between the A-chain helix 2 and the B-chain helix (Figure S4, Supporting Information), two additional docking regions within 5 Å of two A-chain helix 2 atoms were selected: C_γ of Leu13 and Leu16. One of the five initial structures of BSPOTPE and a site were randomly chosen to perform docking with both protein side chains and BSPOTPE hydrophilic tails. The dockings were repeated 1000 times for each of the protein structures. Among the docking poses with lowest energies, those with unreasonable geometries were manually removed.

■ ASSOCIATED CONTENT

⬤ Supporting Information

Changes in the PL intensity of BSPOTPE in the presence and absence of insulin fibrils at different pH and with different salt concentration; experimental procedures for using BSPOTPE as *ex situ* indicator and *in situ* inhibitor; CD spectra of insulin incubated in the presence of different BSPOTPE dose for different periods of time; time-dependent change in ellipticity of insulin; flowchart of theoretic simulations; rmsd plots for the first and second helixes of A chain with B chain helix;

populations of the 100 clusters generated from the k-center clustering algorithm; representative structures from clusters with population >1%; initial conformations of BSPOTPE for docking; docking poses with the lowest energies under fibril forming condition; absorption spectrum of CR in water and emission spectrum of BSPOTPE with insulin fibrils in PBS; emission spectra of BSPOTPE, CR, and BSPOTPE/CR in the presence of insulin fibrils; and complete refs 34, 57, and 79. This material is available free of charge via the Internet at http://pubs.acs.org.

■ AUTHOR INFORMATION

Corresponding Author
xuhuihuang@ust.hk; tangbenz@ust.hk

■ ACKNOWLEDGMENTS

■ REFERENCES

(1) Kelly, J. W. *Curr. Opin. Struct. Biol.* **1998**, *8*, 101.
(2) Stefani, M.; Dobson, C. *J. Mol. Med.* **2003**, *81*, 678.
(3) Sipe, J. D.; Cohen, A. S. *J. Struct. Biol.* **2000**, *130*, 88.
(4) Morris, K.; Serpell, L. *Chem. Soc. Rev.* **2010**, *39*, 3445.
(5) Greenwald, J.; Riek, R. *Structure* **2010**, *18*, 1244.
(6) Dobson, C. M. *Nature* **2003**, *426*, 884.
(7) Hardy, J.; Selkoe, D. J. *Science* **2002**, *297*, 353.
(8) Bernstein, S. L.; Dupuis, N. F.; Lazo, N. D.; Wyttenbach, T.; Condron, M. M.; Bitan, G.; Teplow, D. B.; Shea, J.-E.; Ruotolo, B. T.; Robinson, C. V.; Bowers, M. T. *Nat. Chem.* **2009**, *1*, 326.
(9) Kayed, R.; Head, E.; Thompson, J. L.; McIntire, T. M.; Milton, S. C.; Cotman, C. W.; Glabel, C. G. *Science* **2003**, *300*, 486.
(10) Ivanova, M. I.; Sievers, S. A.; Sawaya, M. R.; Wall, J. S.; Eisenberg, D. *Proc. Natl. Acad. Sci. U.S.A.* **2009**, *106*, 18990.
(11) Dische, F.; Wernstedt, C.; Westermark, G.; Westermark, P.; Pepys, M.; Rennie, J.; Gilbey, S.; Watkins, P. *Diabetologia* **1988**, *31*, 158.
(12) Wilhelm, K. R.; Yanamandra, K.; Gruden, M. A.; Zamotin, V.; Malisauskas, M.; Casaite, V.; Darinskas, A.; Forsgren, L.; Morozova-Roche, L. A. *Eur. J. Neurology* **2007**, *14*, 327.
(13) Sluzky, V.; Tamada, J. A.; Klibanov, A. M.; Langer, R. *Proc. Natl. Acad. Sci. U.S.A.* **1991**, *88*, 9377.
(14) Frokjaer, S.; Otzen, D. E. *Nat. Rev. Drug Discov.* **2005**, *4*, 298.
(15) Blundell, T. L.; Cutfield, J. F.; Dodson, G. G.; Dodson, E.; Hodgkin, D. C.; Mercola, D. *Biochem. J.* **1971**, *125*, 50P.
(16) Brange, J.; Andersen, L.; Laursen, E. D.; Meyn, G.; Rasmussen, E. *J. Pharm. Sci.* **1997**, *86*, 517.
(17) Nielsen, L.; Khurana, R.; Coats, A.; Frokjaer, S.; Brange, J.; Vyas, S.; Uversky, V. N.; Fink, A. L. *Biochemistry* **2001**, *40*, 6036.
(18) Dzwolak, W.; Ravindra, R.; Winter, R. *Phys. Chem. Chem. Phys.* **2004**, *6*, 1938.
(19) Vernaglia, B. A.; Huang, J.; Clark, E. D. *Biomacromolecules* **2004**, *5*, 1362.
(20) Skora, L.; Becker, S.; Zweckstetter, M. *J. Am. Chem. Soc.* **2010**, *132*, 9223.
(21) Rubin, N.; Perugia, E.; Goldschmidt, M.; Fridkin, M.; Addadi, L. *J. Am. Chem. Soc.* **2008**, *130*, 4602.
(22) Nettleton, E. J.; Tito, P.; Sunde, M.; Bouchard, M.; Dobson, C. M.; Robinson, C. V. *Biophys. J.* **2000**, *79*, 1053.
(23) Manno, M.; Craparo, E. F.; Podestà, A.; Bulone, D.; Carrotta, R.; Martorana, V.; Tiana, G.; San Biagio, P. L. *J. Mol. Biol.* **2007**, *366*, 258.
(24) Domike, K. R.; Donald, A. M. *Biomacromolecules* **2007**, *8*, 3930.
(25) Pratim Bose, P.; Chatterjee, U.; Xie, L.; Johansson, J.; Göthelid, E.; Arvidsson, P. I. *ACS Chem. Neurosci.* **2010**, *1*, 315.
(26) Levine, H. *Protein Sci.* **1993**, *2*, 404.
(27) Groenning, M.; Norrman, M.; Flink, J. M.; van de Weert, M.; Bukrinsky, J. T.; Schluckebier, G.; Frokjaer, S. *J. Struct. Biol.* **2007**, *159*, 483.
(28) Rodriguez-Rodriguez, C.; Rimola, A.; Rodriguez-Santiago, L.; Ugliengo, P.; Alvarez-Larena, A.; Gutierrez-de-Teran, H.; Sodupe, M.; Gonzalez-Duarte, P. *Chem. Commun.* **2010**, *46*, 1156.
(29) Bekard, I. B.; Dunstan, D. E. *Biophys. J.* **2009**, *97*, 2521.
(30) Herland, A.; Nilsson, K. P. R; Olsson, J. D. M.; Hammarström, P.; Konradsson, P.; Inganäs, O. *J. Am. Chem. Soc.* **2005**, *127*, 2317.
(31) Kitts, C. C.; Beke-Somfai, T. s.; Nordén, B. *Biochemistry* **2011**, *50*, 3451.
(32) Nesterov, E. E.; Skoch, J.; Hyman, B. T.; Klunk, W. E.; Bacskai, B. J.; Swager, T. M. *Angew. Chem., Int. Ed.* **2005**, *44*, 5452.
(33) Liang, Y.; Lynn, D. G.; Berland, K. M. *J. Am. Chem. Soc.* **2010**, *132*, 6306.
(34) Åslund, A.; et al. *ACS Chem. Biol.* **2009**, *4*, 673.
(35) Åslund, A.; Herland, A.; Hammarström, P.; Nilsson, K. P. R; Jonsson, B.-H.; Inganäs, O.; Konradsson, P. *Bioconjugate Chem.* **2007**, *18*, 1860.
(36) Ran, C.; Xu, X.; Raymond, S. B.; Ferrara, B. J.; Neal, K.; Bacskai, B. J.; Medarova, Z.; Moore, A. *J. Am. Chem. Soc.* **2009**, *131*, 15257.
(37) Chang, W. M.; Dakanali, M.; Capule, C. C.; Sigurdson, C. J.; Yang, J.; Theodorakis, E. A. *ACS Chem. Neurosci.* **2011**, *2*, 249.
(38) Roberti, M. J.; Morgan, M.; Menéndez, G.; Pietrasanta, L. a. I.; Jovin, T. M.; Jares-Erijman, E. A. *J. Am. Chem. Soc.* **2009**, *131*, 8102.
(39) Luo, J.; Xie, Z.; Lam, J. W. Y.; Cheng, L.; Chen, H.; Qiu, C.; Kwok, H. S.; Zhan, X.; Liu, Y.; Zhu, D.; Tang, B. Z. *Chem. Commun.* **2001**, 1740.
(40) (a) Hong, Y.; Lam, J. W. Y.; Tang, B. Z. *Chem. Commun.* **2009**, 4332. (b) Hong, Y.; Lam, J. W. Y.; Tang, B. Z. *Chem. Soc. Rev.* **2011**, *40*, 5361.
(41) (a) Qin, A.; Lam, J. W. Y.; Tang, B. Z. *Prog. Polym. Sci.* **2012**, *37*, 182. (b) Liu, J.; Lam, J.; Tang, B. Z. *J. Inorg. Organomet. Polym. Mater.* **2009**, *19*, 249.
(42) (a) Zhao, Z.; Lam, J. W. Y.; Tang, B. Z. *Curr. Org. Chem.* **2010**, *14*, 2109. (b) Wang, M.; Zhang, G.; Zhang, D.; Zhu, D.; Tang, B. Z. *J. Mater. Chem.* **2010**, *20*, 1858.
(43) Nilsson, K. P. R *FEBS Lett.* **2009**, *583*, 2593.
(44) Carter, M. D.; Simms, G. A.; Weaver, D. F. *Clin. Pharmacol. Ther.* **2010**, *88*, 475.
(45) Bohrmann, B.; Adrian, M.; Dubochet, J.; Kuner, P.; Müller, F.; Huber, W.; Nordstedt, C.; Döbeli, H. *J. Struct. Biol.* **2000**, *130*, 232.
(46) Murray, M. M.; Bernstein, S. L.; Nyugen, V.; Condron, M. M.; Teplow, D. B.; Bowers, M. T. *J. Am. Chem. Soc.* **2009**, *131*, 6316.
(47) Takahashi, T.; Mihara, H. *Acc. Chem. Res.* **2008**, *41*, 1309.
(48) Giger, K.; Vanam, R. P.; Seyrek, E.; Dubin, P. L. *Biomacromolecules* **2008**, *9*, 2338.
(49) Cabaleiro-Lago, C.; Quinlan-Pluck, F.; Lynch, I.; Dawson, K. A.; Linse, S. *ACS Chem. Neurosci.* **2010**, *1*, 279.
(50) Yoo, S. I.; Yang, M.; Brender, J. R.; Subramanian, V.; Sun, K.; Joo, N. E.; Jeong, S.-H.; Ramamoorthy, A.; Kotov, N. A. *Angew. Chem., Int. Ed.* **2011**, *50*, 5110.
(51) Man, B. Y.-W.; Chan, H.-M.; Leung, C.-H.; Chan, D. S.-H.; Bai, L.-P.; Jiang, Z.-H.; Li, H.-W.; Ma, D.-L. *Chem. Sci.* **2011**, *2*, 917.
(52) Geng, J.; Li, M.; Ren, J.; Wang, E.; Qu, X. *Angew. Chem., Int. Ed.* **2011**, *50*, 4184.
(53) Yamin, G.; Ruchala, P.; Teplow, D. B. *Biochemistry* **2009**, *48*, 11329.
(54) Sievers, S. A.; Karanicolas, J.; Chang, H. W.; Zhao, A.; Jiang, L.; Zirafi, O.; Stevens, J. T.; Munch, J.; Baker, D.; Eisenberg, D. *Nature* **2011**, *475*, 96.
(55) Arora, A.; Ha, C.; Park, C. B. *FEBS Lett.* **2004**, *564*, 121.
(56) Levy-Sakin, M.; Shreberk, M.; Daniel, Y.; Gazit, E. *Islets* **2009**, *1*, 210.
(57) Kukar, T. L.; et al. *Nature* **2008**, *453*, 925.

(58) Chen, J.; Armstrong, A. H.; Koehler, A. N.; Hecht, M. H. *J. Am. Chem. Soc.* **2010**, *132*, 17015.

(59) Soto-Ortega, D. D.; Murphy, B. P.; Gonzalez-Velasquez, F. J.; Wilson, K. A.; Xie, F.; Wang, Q. A.; Moss, M. A. *Bioorg. Med. Chem.* **2011**, *19*, 2596.

(60) Reinke, A. A.; Gestwicki, J. E. *Chem. Biol. Drug Des.* **2007**, *70*, 206.

(61) Heldt, C. L.; Sorci, M.; Posada, D.; Hirsa, A.; Belfort, G. *Biotechnol. Bioeng.* **2011**, *108*, 237.

(62) Smith, M. I.; Sharp, J. S.; Roberts, C. J. *Biophys. J.* **2008**, *95*, 3400.

(63) Bolognesi, B.; Kumita, J. R.; Barros, T. P.; Esbjorner, E. K.; Luheshi, L. M.; Crowther, D. C.; Wilson, M. R.; Dobson, C. M.; Favrin, G.; Yerbury, J. J. *ACS Chem. Biol.* **2010**, *5*, 735.

(64) Hong, Y.; Feng, C.; Yu, Y.; Liu, J.; Lam, J. W. Y.; Luo, K. Q.; Tang, B. Z. *Anal. Chem.* **2010**, *82*, 7035.

(65) Tong, H.; Hong, Y.; Dong, Y.; Häussler, M.; Li, Z.; Lam, J. W. Y.; Dong, Y.; Sung, H. H. Y.; Williams, I. D.; Tang, B. Z. *J. Phys. Chem. B* **2007**, *111*, 11817.

(66) Groenning, M. *J. Chem. Biol.* **2010**, *3*, 1.

(67) Choi, J. H.; May, B. C. H.; Wille, H.; Cohen, F. E. *Biophys. J.* **2009**, *97*, 3187.

(68) Sawaya, M. R.; Sambashivan, S.; Nelson, R.; Ivanova, M. I.; Sievers, S. A.; Apostol, M. I.; Thompson, M. J.; Balbirnie, M.; Wiltzius, J. J. W.; McFarlane, H. T.; Madsen, A. O.; Riekel, C.; Eisenberg, D. *Nature* **2007**, *447*, 453.

(69) Meiler, J.; Baker, D. *Proteins* **2006**, *65*, 538.

(70) Davis, I. W.; Baker, D. *J. Mol. Biol.* **2009**, *385*, 381.

(71) Devlin, G. L.; Knowles, T. P. J; Squires, A.; McCammon, M. G.; Gras, S. L.; Nilsson, M. R.; Robinson, C. V.; Dobson, C. M.; MacPhee, C. E. *J. Mol. Biol.* **2006**, *360*, 497.

(72) Turnell, W. G.; Finch, J. T. *J. Mol. Biol.* **1992**, *227*, 1205.

(73) Porat, Y.; Abramowitz, A.; Gazit, E. *Chem. Biol. Drug Des.* **2006**, *67*, 27.

(74) Sugita, Y.; Okamoto, Y. *Chem. Phys. Lett.* **1999**, *314*, 141.

(75) Hansmann, U. H. E. *Chem. Phys. Lett.* **1997**, *281*, 140.

(76) McWeeny, R.; Diercksen, G. *Self Consistent Perturbation Theory. II. Extension to Open Shells*; AIP: 1968; Vol. *49*.

(77) Pople, J. A.; Nesbet, R. K. *J. Chem. Phys.* **1954**, *22*, 571.

(78) Roothaan, C. C. J. *Rev. Mod. Phys.* **1951**, *23*, 69.

(79) Frisch, M. J.; et al. *Gaussian 03*, Revision B.01; Gaussian, Inc.: Pittsburgh, PA, 2003.

(80) Hornak, V.; Abel, R.; Okur, A.; Strockbine, B.; Roitberg, A.; Simmerling, C. *Proteins* **2006**, *65*, 712.

(81) Hess, B.; Kutzner, C.; van der Spoel, D.; Lindahl, E. *J. Chem. Theory Comput.* **2008**, *4*, 435.

(82) Jorgensen, W. L.; Chandrasekhar, J.; Madura, J. D.; Impey, R. W.; Klein, M. L. *J. Chem. Phys.* **1983**, *79*, 926.

(83) Berendsen, H. J. C.; Postma, J. P. M; Vangunsteren, W. F.; Dinola, A.; Haak, J. R. *J. Chem. Phys.* **1984**, *81*, 3684.

(84) Bussi, G.; Donadio, D.; Parrinello, M. *J. Chem. Phys.* **2007**, *126*, No. 014101.

(85) Essmann, U.; Perera, L.; Berkowitz, M. L.; Darden, T.; Lee, H.; Pedersen, L. G. *J. Chem. Phys.* **1995**, *103*, 8577.

(86) Darden, T.; York, D.; Pedersen, L. *J. Chem. Phys.* **1993**, *98*, 10089.

(87) Hess, B.; Bekker, H.; Berendsen, H. J. C.; Fraaije, J. G. E. M. *J. Comput. Chem.* **1997**, *18*, 1463.

(88) Huang, X.; Bowman, G. R.; Pande, V. S. *J. Chem. Phys.* **2008**, *128*, 205106.

(89) Bowman, G. R.; Huang, X.; Pande, V. S. *Methods* **2009**, *49*, 197.

(90) Meiler, J.; Baker, D. *Proteins* **2006**, *65*, 538.

(91) Baker, D.; Davis, I. W. *J. Mol. Biol.* **2009**, *385*, 381.

(92) Gray, J. J.; Moughon, S.; Wang, C.; Schueler-Furman, O.; Kuhlman, B.; Rohl, C. A.; Baker, D. *J. Mol. Biol.* **2003**, *331*, 281.

(93) Jakalian, A.; Jack, D. B.; Bayly, C. I. *J. Comput. Chem.* **2002**, *23*, 1623.

(94) Jakalian, A.; Bush, B. L.; Jack, D. B.; Bayly, C. I. *J. Comput. Chem.* **2000**, *21*, 132.